Available online at www.eccomasproceedia.org
Eccomas Proceedia COMPDYN (2021) 4607-4620

ECCOMAS
Proceedia

COMPDYN 2021
8th ECCOMAS Thematic Conference on
Computational Methods in Structural Dynamics and Earthquake Engineering
M. Papadrakakis, M. Fragiadakis (eds.)
Streamed from Athens, Greece, 28 - 30 June 2021

SEISMIC RELIABILITY OF BRIDGES ISOLATED WITH FPS

P. Castaldo[1], G. Amendola[2], L. Giordano[2], D. Gino[2], and E. Miceli[2]

[1] Department of Structural, Geotechnical and Building Engineering (DISEG), Politecnico di Torino, Turin, Italy
e-mail: paolo.castaldo@polito.it ; pcastaldo@unisa.it

[2] Department of Structural, Geotechnical and Building Engineering (DISEG), Politecnico di Torino, Turin, Italy
{guglielmo.amendola, luca.giordano, diego.gino, elena.miceli}@polito.it

Abstract

The present analysis deals with the seismic reliability of isolated multi-span continuous deck bridges considering as the main aleatory uncertainties relevant to the problem the sliding friction coefficient of the friction pendulum (FP) isolators together with the seismic records characteristics. A six-degree-of-freedom model is defined to simulate the elastic response of the reinforced concrete pier, the infinitely rigid response of the deck supported by the seismic devices and the non-linear velocity-dependent behavior of the FPS bearings. The reinforced concrete abutment is modelled as a rigid support above which a FPS device is located. A set of natural records with different characteristics is properly selected and scaled to increasing intensity levels. The randomness on the friction coefficient is described by an appropriate probability density function to sample. For different system and isolator properties, fragility curves of both the reinforced concrete pier and FP devices supporting the deck are estimated. In accordance with the hazard curve of the design site, the seismic reliability curves are derived by means of the convolution integral.

Keywords: Seismic isolation, Bridge, Friction pendulum isolators, Performance-based engineering, Seismic reliability.

ISSN:2623-3347
Peer-review under responsibility of the organizing committee of COMPDYN 2021.
doi: 10.7712/120121.8811.18550

1 INTRODUCTION

The aim of seismic isolation for bridges is to uncouple the deck from the horizontal components of the earthquake action, allowing a significant reduction of both acceleration and forces transmitted from the deck to the pier, compared to non-isolated bridges, as demonstrated in [1]-[3]. This topic is very crucial to the issue of the infrastructure safety [4]-[5]. Among the possible seismic retrofitting solutions, single concave friction pendulum system (FPS) devices have been often used because they imply a high dissipation capacity and determine an isolation period independent of the isolated mass as well as for their durability properties [6]-[10].

The use of both elastomeric and FPS bearings is studied in [11], where the efficacy of using simplified models in relation to the flexibility of the deck and of the piers is emphasized. Optimal values for the friction coefficient in seismic isolated bridges are proposed in [12], as function of the structural properties and of the soil condition. Furthermore, a three-dimensional multi-span continuous steel girder bridge, isolated by FPS isolators, is studied in [13], where the effect of modeling parameters and the influence of the design parameters on the response is investigated.

Seismic reliability-based design (SRBD) approach has been proposed in [14]-[18], in the context of investigating new design solutions for these seismic devices in relation to their main uncertainties. In [19] it is presented a probability-based reliability assessment method to consider the variations of the seismic isolation properties under different conditions, referring to a base-isolated two span reinforced concrete (RC) bridge. Seismic reliability analysis of a multi-span bridge pier developed through the response surface method-based metamodeling approach is described in [20]. Different methodologies to deal with seismic fragility assessment of highway bridges is presented in [21]. The research by [22] regards the efficiency of numerous seismic intensity measures to estimate the response of seismic-isolated bridges in relation to ordinary and pulse-like ground motions. Life-cycle reliability analyses of RC bridges are presented in [23]. In [24], the seismic design of RC bridge structures in relation to both ductile and brittle resisting mechanisms is evaluated, by proposing a reliability-based analysis with partial factors.

The present study regards the seismic reliability of multi-span continuous deck bridges isolated with FPS devices through the analysis of fragility curves related to a wide range of bridge properties as well as different seismic intensity levels. Five-degree-of-freedom (dof) models have been adopted, accounting for five vibrational modes representative of the elastic RC pier behaviour and another dof is added to analyze the response of the infinitely rigid RC deck isolated by the FPS devices. The pier-abutment-deck interaction is taken into account by modelling the RC abutment as a rigid support [2],[25],[26]. To model the behaviour of the FPS device the hypothesis of the friction coefficient varying with the velocity is adopted, as proposed by [7]. The friction coefficient has been described by means of an appropriate normal probability density function (PDF) and the Latin hypercube Sampling Method (LHS) [27], is employed as the random sampling technique to define the set of the input data. In addition, seismic uncertainty is accounted by considering 30 natural seismic records with different characteristics, scaled to different increasing intensity levels in line with the seismic hazard of the reference site (i.e., L'Aquila (Italy)). The relation between seismic demand and the capacity of the isolated bridge is analyzed through incremental dynamic analyses (IDAs) [28].Thus, the response statistics related to both the superstructure (i.e., deck) and the pier have been evaluated. For the former in terms of peak deck displacement (with respect to the pier) and for the latter in terms of peak pier displacement (with respect to the ground). Furthermore, the results regarding the response statistics have been used to evaluate the seismic fragility curves

of both the rigid deck and the RC pier, assuming appropriate values of the corresponding limit state thresholds. The above-mentioned analyses (i.e., fragility curves) have been useful to assess the seismic reliability of bridges isolated with FPS bearings, according to the PEER-like modular approach [29], assuming the hazard curves of the site and a specific design life.

2 EQUATIONS OF MOTION

The structural system of an isolated multi-span continuous deck bridge is modelled, according to [2],[25],[26], as the sum of 5dof corresponding to the lumped masses of the RC pier and 1dof related to the rigid RC deck mass. The RC abutment is modeled as rigid and fixed.

The equations of motion of the response of an isolated bridge on FPS devices subjected to the seismic input along the longitudinal direction, $\ddot{u}_g(t)$, are:

$$\begin{aligned}
&m_d\ddot{u}_d(t)+m_d\ddot{u}_{p5}(t)+m_d\ddot{u}_{p4}(t)+m_d\ddot{u}_{p3}(t)+m_d\ddot{u}_{p2}(t)+m_d\ddot{u}_{p1}(t)+c_d\dot{u}_d(t)+f_b(t)+f_a(t)=-m_d\ddot{u}_g(t)\\
&m_{p5}\ddot{u}_{p5}(t)+m_{p5}\ddot{u}_{p4}(t)+m_{p5}\ddot{u}_{p3}(t)+m_{p5}\ddot{u}_{p2}(t)+m_{p5}\ddot{u}_{p1}(t)-c_d\dot{u}_d(t)+c_{p5}\dot{u}_{p5}(t)+k_{p5}u_{p5}(t)-f_b(t)=-m_{p5}\ddot{u}_g(t)\\
&m_{p4}\ddot{u}_{p4}(t)+m_{p4}\ddot{u}_{p3}(t)+m_{p4}\ddot{u}_{p2}(t)+m_{p4}\ddot{u}_{p1}(t)-c_{p5}\dot{u}_{p5}(t)-k_{p5}u_{p5}(t)+c_{p4}\dot{u}_{p4}(t)+k_{p4}u_{p4}(t)=-m_{p4}\ddot{u}_g(t)\\
&m_{p3}\ddot{u}_{p3}(t)+m_{p3}\ddot{u}_{p2}(t)+m_{p3}\ddot{u}_{p1}(t)-c_{p4}\dot{u}_{p4}(t)-k_{p4}u_{p4}(t)+c_{p3}\dot{u}_{p3}(t)+k_{p3}u_{p3}(t)=-m_{p3}\ddot{u}_g(t)\\
&m_{p2}\ddot{u}_{p2}(t)+m_{p2}\ddot{u}_{p1}(t)-c_{p3}\dot{u}_{p3}(t)-k_{p3}u_{p3}(t)+c_{p2}\dot{u}_{p2}(t)+k_{p2}u_{p2}(t)=-m_{p2}\ddot{u}_g(t)\\
&m_{p1}\ddot{u}_{p1}(t)-c_{p2}\dot{u}_{p2}(t)-k_{p2}u_{p2}(t)+c_{p1}\dot{u}_{p1}(t)+k_{p1}u_{p1}(t)=-m_{p1}\ddot{u}_g(t)
\end{aligned} \tag{1}$$

where u_d represents the horizontal displacement of the deck relative to the pier, $u_{p,i}$ the displacement of the *i*-th ($i=1:5$) pier mass relative to the *i*-th-1 dof, m_d and m_{pi} are respectively the mass of the deck and of the *i*-th ($i=1:5$) lumped mass of the pier, c_d is the viscous damping constant of the isolated deck, k_{pi} and c_{pi} respectively the pier stiffness and inherent viscous damping constant of the *i*-th ($i=1:5$) dof of the pier, *t* the time instant, $f_a(t)$ and $f_p(t)$ are the reactions of the FP bearings, respectively on the abutment and on the pier, equal to:

$$f_a(t)=\frac{m_d g}{2R}\left(u_d(t)+\sum_{i=1}^{5}u_{pi}\right)+\frac{1}{2}\left(\mu_a\left(\dot{u}_d(t)+\sum_{i=1}^{5}\dot{u}_{pi}\right)\right)m_d g\left(\operatorname{sgn}\left(\dot{u}_d(t)+\sum_{i=1}^{5}\dot{u}_{pi}\right)\right) \tag{2}$$

$$f_p(t)=\frac{m_d g u_d(t)}{2R}+\frac{\mu_p(\dot{u}_d)\,m_d g\operatorname{sgn}(\dot{u}_d)}{2} \tag{3}$$

where g is the gravity constant, *R* is the radius of curvature of the two FPS isolators assumed equal, $\mu(\dot{u}(t))$ represents the sliding friction coefficient of the isolator on the abutment (subscript *a*) or of the isolator on the pier (subscript *p*), which depends on the bearing slip velocity $\dot{u}(t)$ (that is a relative velocity with respect to the ground for the isolator on the abutment or to the pier top for the isolator on the pier), and *sgn*(·) denotes the sign function.

Regarding Equations (2)-(3), the first addenda represent the elastic behaviour ($k_d=m_d g/R$), associated to the pendulum motion with fundamental vibration period equal to $T_d=2\pi\sqrt{R/g}$ (i.e., only function of the radius of curvature *R*), and the second is the frictional behaviour, related to the sliding friction coefficient of the teflon-steel interface [14]. Experimental results

[7]-[9] suggest adopting the following equation to model the sliding friction coefficient of teflon-steel interfaces:

$$\mu\left(\dot{u}\right) = f_{\max} - \left(f_{\max} - f_{\min}\right) \cdot \exp\left(-\alpha\left|\dot{u}\right|\right) \tag{4}$$

where $f_{\max}$ is the maximum value of friction coefficient at large sliding velocities, and $f_{\min}$ represents the value at zero velocity. Considering this, the hypothesis of continuous sliding in structures supported by teflon bearings is included by assuming, for simplicity, a ratio $f_{\max} / f_{\min}$ equal to 3 and an exponent α equal to 30, based on a regression of the experimental results of [7]-[9].

Note that cracking phenomena [30]-[34] of the RC deck are herein neglected.

3 ALEATORY UNCERTAINTIES AND DETERMINISTIC PARAMETERS

The relevant uncertainties assumed in the following parametric study are presented in this section. In particular, the seismic performance of multi-span continuous deck bridges isolated with FP bearings is evaluated for different structural properties, assumed as deterministic parameters.

3.1 Seismic records

The uncertainties regarding the seismic input intensity are separated from the ones related to the characteristics of the record (i.e., record-to-record variability), according to the performance-based earthquake engineering (PBEE) approach [35],[36]. Specifically, a scale factor, i.e., an intensity measure (*IM)*, is considered such that the randomness in the seismic intensity is described by a hazard curve while the ground motion randomness for a fixed intensity level can be represented by a set of ground motions with a different duration and frequency content, scaled according to *IM*. A set of 30 natural ground motion records are considered in this work, selected from [37]-[39], in line with [40]. Particularly, these records derive from 19 different seismic events. The largest source-to-site distance is 98.2km, the moment magnitude (M) varies between 6.0 and 7.6, the PGA between 0.13g and 0.94g. Table 1 illustrates the main properties of these earthquakes.

	Year	Earthquake Name	Recording Station Name	Vs_{30} [m/sec]	Source (Fault Type)	M [-]	R [km]	PGA_{max} [g]
1	1994	Northridge	Beverly Hills - Mulhol	356	Thrust	6.7	13.3	0.52
2	1994	Northridge	Canyon Country-WLC	309	Thrust	6.7	26.5	0.48
3	1994	Northridge	LA – Hollywood Stor	316	Thrust	6.7	22.9	0.36
4	1999	Duzce, Turkey	Bolu	326	Strike-slip	7.1	41.3	0.82
5	1999	Hector Mine	Hector	685	Strike-slip	7.1	26.5	0.34
6	1979	Imperial Valley	Delta	275	Strike-slip	6.5	33.7	0.35
7	1979	Imperial Valley	El Centro Array #11	196	Strike-slip	6.5	29.4	0.38
8	1995	Kobe, Japan	Nishi-Akashi	609	Strike-slip	6.9	8.7	0.51
9	1995	Kobe, Japan	Shin-Osaka	256	Strike-slip	6.9	46	0.24
10	1999	Kocaeli, Turkey	Duzce	276	Strike-slip	7.5	98.2	0.36
11	1999	Kocaeli, Turkey	Arcelik	523	Strike-slip	7.5	53.7	0.22
12	1992	Landers	Yermo Fire Station	354	Strike-slip	7.3	86	0.24
13	1992	Landers	Coolwater	271	Strike-slip	7.3	82.1	0.42
14	1989	Loma Prieta	Capitola	289	Strike-slip	6.9	9.8	0.53
15	1989	Loma Prieta	Gilroy Array #3	350	Strike-slip	6.9	31.4	0.56
16	1990	Manjil, Iran	Abbar	724	Strike-slip	7.4	40.4	0.51
17	1987	Superstition Hills	El Centro Imp. Co.	192	Strike-slip	6.5	35.8	0.36
18	1987	Superstition Hills	Poe Road (temp)	208	Strike-slip	6.5	11.2	0.45

19	1987	Superstition Hills	Westmorland Fire Stat.	194	Strike-slip	6.5	15.1	0.21
20	1992	Cape Mendocino	Rio Dell Overpass	312	Thrust	7.0	22.7	0.55
21	1999	Chi-Chi, Taiwan	CHY101	259	Thrust	7.6	32	0.44
22	1999	Chi-Chi, Taiwan	TCU045	705	Thrust	7.6	77.5	0.51
23	1971	San Fernando	LA - Hollywood Stor	316	Thrust	6.6	39.5	0.21
24	1976	Friuli, Italy	Tolmezzo	425	Thrust	6.5	20.2	0.35
25	1980	Irpinia	Bisaccia	496		6.9	21.3	0.94
26	1979	Montenegro	ST64	1083	Thrust	6.9	21.0	0.18
27	1997	Umbria Marche	ST238	n/a	Normal	6.0	21.5	0.19
28	2000	South Iceland	ST2487	n/a	Strike-slip	6.5	13	0.16
29	2000	South Iceland (a.s.)	ST2557	n/a	Strike-slip	6.5	15.0	0.13
30	2003	Bingol	ST539	806	Strike-slip	6.3	14.0	0.30

Table 1: Selected ground motions for the time history analysis.

3.2 Intensity measure in terms of spectral displacement

According to [41]-[44], the selection of the intensity measure should follow the criteria of efficiency, sufficiency and hazard compatibility. For the case of this work, the *IM* is chosen as the spectral-displacement $S_D\left(T_d,\xi_d\right)$ which corresponds to the isolated period of the bridge system, $T_d = 2\pi/\omega_d$, and for the damping ratio ξ_d. As demonstrated in many studies, e.g., [41]-[43],[45], not only the spectral-displacement is more efficient than the peak ground acceleration, but also its use allows to obtain more reliable response estimates for a given number of records and to reduce the response dispersion [22].

In line with other studies [22], the damping ratio ξ_d is assumed equal to zero [46]. Therefore, in the following, the corresponding *IM* is indicated as $S_D\left(T_d\right)$ and, to compute the IDAs, it is assumed varying from 0.10m to 0.45m (Table 2) in compliance with the seismic hazard of the reference site (L'Aquila (Italy)), from the operational to collapse limit state, as provided by [44].

IM	1	2	3	4	5	6	7	8
$S_D(T_d)$ [m]	0.10	0.15	0.20	0.25	0.30	0.35	0.40	0.45

Table 2: Selected values of the intensity measure $S_D(T_d)$.

3.3 Random variable of the friction coefficient

According to the experimental data on sheet-type teflon bearings [7]-[9], friction is not constant during sliding, as stated in the friction Coulomb law, but it is a much more complex phenomenon, governed by different mechanisms such as the sliding velocity, apparent pressure and temperature. Moreover, it has also been observed by [47] that the friction coefficient varies in space. That is why the sliding friction coefficient at large velocity $f_{\max}$ is considered as a random variable described by a truncated normal PDF, with an average equal to 3%, a minimum value of 0.5% and a maximum of 5.5% as also studied in [14],[17],[18]. Furthermore, being valid the relation $f_{\min} = f_{\max}/3$, the values of the friction coefficient at the low velocities, $f_{\min}$, have also been assumed as random variables. Finally, α is considered equal to a deterministic value of 30 [17] (Equation (4)).

To deal with the abovementioned random variables, the LHS method [17] has been used to generate the input data samples starting from their PDFs, with a sample number of 15.

3.4 Deterministic structural properties

A parametric analysis has been conducted in this work, which has brought to a set of different isolated bridge models. Specifically, in compliance with [15],[25],[26],[46], the parameters ξ_d and $\xi_{pi} = \xi_p$ are assumed respectively equal to 0% and 5%; the isolated deck period T_d is in the range between 1s and 4s; the RC pier period T_p equal to 0.2s; the overall mass ratio $\lambda = \sum_{i=1,5} m_{pi} / m_d$ that is related to the sum of the *i*-th mass ratios (assumed equal), is in the range between 0.1, 0.15 and 0.2.

Combining these deterministic values with the above sampled values of the friction coefficient, 90 different types of isolated bridges are defined.

4 INCREMENTAL DYNAMIC ANALYSIS RESULTS FOR THE DIFFERENT STRUCTURAL PROPERTIES

The differential equations of motion (Equation (1)) have been solved for each of the 90 bridge models, combining the deterministic (T_d, λ and T_p) and aleatory parameters and for the 30 different ground motion records (Table 1), scaled to the increasing 8 values of $S_D(T_d)$ (Table 2). Thus, IDAs [28] are performed in MATLAB-Simulink [48] employing the Runge-Kutta-Fehlberg integration algorithm. For each of the 90 deterministic combinations, a total number of 450 simulations has been carried out by pairing each one of the 30 seismic records with the sampled 15 friction coefficients. The IDAs have been obtained assuming the following engineering demand parameters (EDPs): the deck response with respect to the pier top u_d and the response of the pier top with respect to the ground u_p, computed as $u_p = \sum_{i=1}^{5} u_{pi}$. For all the engineering demand parameters, the peak responses are determined: $u_{d,\max}$ and $u_{p,\max} = \left| \left(\sum_{i=1}^{5} u_{pi} \right) \right|_{\max}$. Following an assumption widely used in PBEE [36], each EDP output has been probabilistically [49]-[56] treated by means of a lognormal PDF: using the maximum likelihood technique [14]-[18], the sample lognormal mean $\mu_{\ln}(EDP)$ and standard deviation $\sigma_{\ln}(EDP)$ are computed for each EDP. In the end, the 50^{th}, 84^{th} and 16^{th} percentiles of each lognormal PDF can be easily evaluated [17].

The following figures show the IDA curves for the peak deck displacement at the pier $u_{d,\max}$ (Figure 1) and for the peak pier displacement $u_{p,\max}$ (Figure 2). In particular, the EDPs values are plotted with respect to the *IM* and each curve corresponds to different percentiles and λ values.

The deck response (Figure 1) tends to decrease for lower values of λ. For the seismic device, the lognormal mean of the isolation system response increases with lower values of T_d, because the lower the period the larger the response, due to resonance phenomena occurring between deck and pier.

Regarding the IDA curves related to the pier response (Figure 2), the structural response generally decreases with increasing T_d due to the effectiveness of the isolation technique. The influence of λ decreases as T_d increases, while the opposite trend regards the dispersion.

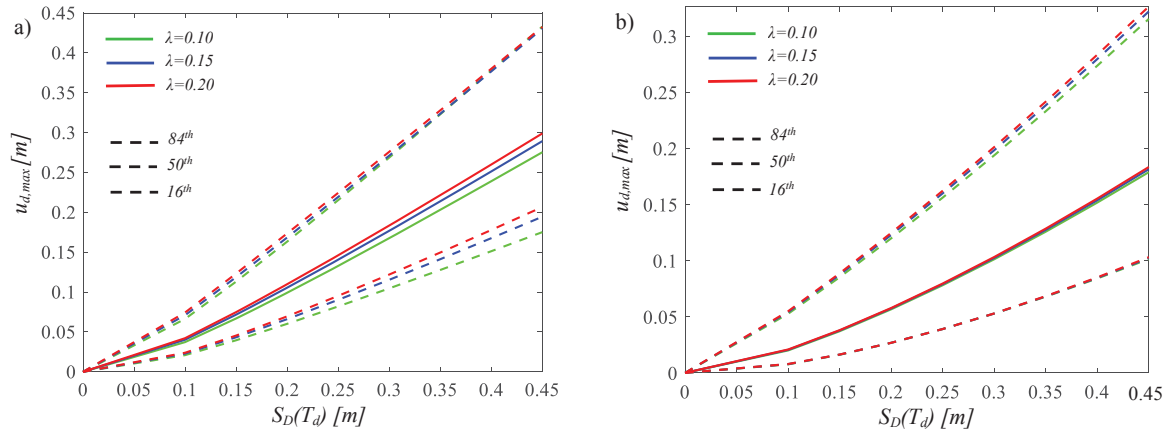

Figure 1: IDA curves of the deck response with respect to the pier, for T_p=0.20s and T_d =1s (a), T_d =4s (b).

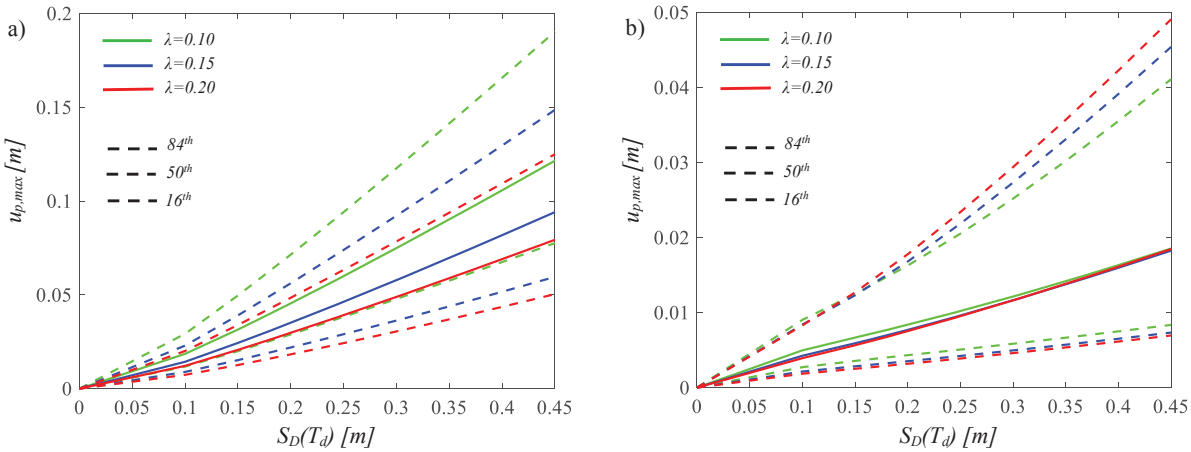

Figure 2: IDA curves of the pier, for T_p=0.20s and T_d =1s (a), T_d =4s (b).

5 SEISMIC FRAGILITY ASSESSMENT

The seismic fragility curves represent the probabilities P_f of exceeding different limit states (*LSs*) conditioned to each level of the *IM*. This implies the need of defining the *LS* threshold related to the isolation system. In particular, nine different values of the in-plan radius for the single concave surface have been assumed [14], herein summed in Table 3.

	1	2	3	4	5	6	7	8	9
r[m]	0.10	0.15	0.20	0.25	0.30	0.35	0.40	0.45	0.50

Table 3: Limit State thresholds for the isolation system.

		PDI	PDI_{IB}	P_f
LS1	Fully Operational	PDI=0.7%	PDI_{IB}=0.23%	$5 \cdot 10^{-1}$
LS2	Operational	PDI=1.5%	PDI_{IB}=0.5%	$1.6 \cdot 10^{-1}$
LS3	Life Safety	PDI=2.5%	PDI_{IB}=0.83%	$2.2 \cdot 10^{-2}$
LS4	Near collapse	PDI=5%	PDI_{IB}=1.67%	$1.5 \cdot 10^{-3}$

Table 4: Limit State thresholds for the pier [58].

Regarding the RC pier, four discrete performance levels or *LSs* (*LS1*, *LS2*, *LS3* and *LS4*), corresponding respectively to "fully operational", "operational", "life safety" and "collapse prevention", are suggested by Vision 2000 [57]. According to the displacement-based seismic

design, the pier drift index (PDI), considered as the measurable structural response parameter, is adopted to define the specific LS threshold related to an acceptable probability of exceeding that LS [14]-[18], or failure probability, in the design/reference life of a structural system. In particular, the performance LSs for isolated bridges, in terms of PDI_{IB}, is defined as 1/3 of the PDI limit value of a comparable non-isolated bridge, in agreement with FEMA provisions [58]. In the following (Table 4), the LS thresholds are presented, together with the failure probabilities to respect in 50 years [14]-[18].

From the fundamental period of the RC pier, T_p, it is finally possible to compute its height [1], needed to assess the seismic fragility of the bridge, as follows:

$$T_p = \frac{2\pi}{(1.875)^2} \cdot \sqrt{\frac{\overline{m}_p h^4}{EI}} \tag{5}$$

where $\overline{m}_p$ is the mass per unit length of the pier, h is its height and EI the flexural rigidity, having assumed a circular cross-section.

5.1 Seismic fragility curves

The probabilities P_f exceeding the LS thresholds have been numerically computed. Then, lognormal complementary cumulative distribution functions (CCDFs), representing the seismic fragility curves, have been fitted with R-square values higher than 0.8 [14],[17].

The results represented in Figure 3-Figure 4 show the fragility curves for T_p =0.2s and the different values assumed for T_d, for each LS and each value of λ, referring to the deck response with respect to the pier and to the RC pier. As a general behaviour, the seismic fragility decreases for larger values of LS thresholds. In addition, in compliance with the previous results (i.e., IDA curves), when the isolated vibration T_d increases, the seismic fragility decreases.

For what concerns the response of the isolation system (Figure 3), the variability of λ causes slight deviations, which are more relevant when T_d is low. In particular, an increase in λ determines an increase in the isolation response relative to the pier.

Regarding the seismic fragility curves for the pier (Figure 4) a larger influence of the λ variability is present, showing a lower fragility when λ increases.

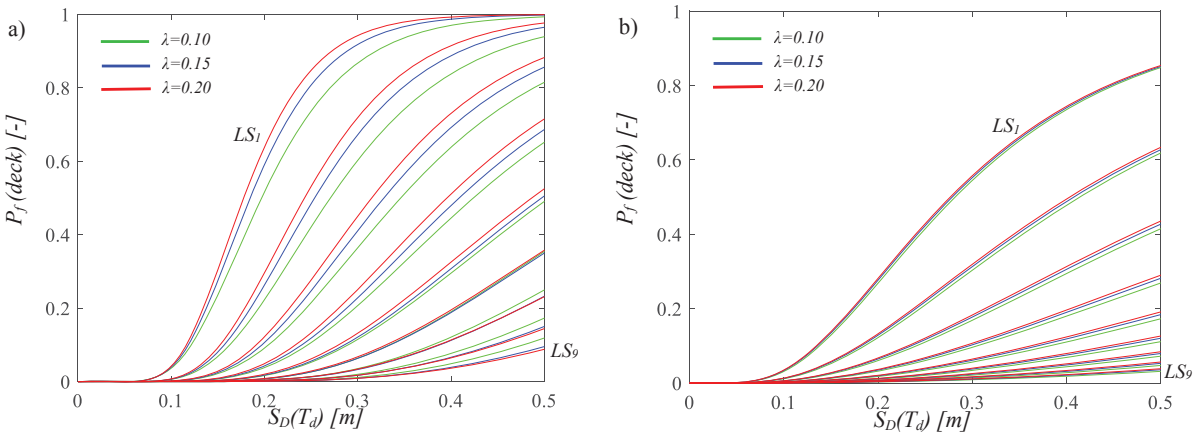

Figure 3: Seismic fragility curves of the deck response with respect to the pier for T_p=0.20s and T_d=1s (a), T_d=4s (b).

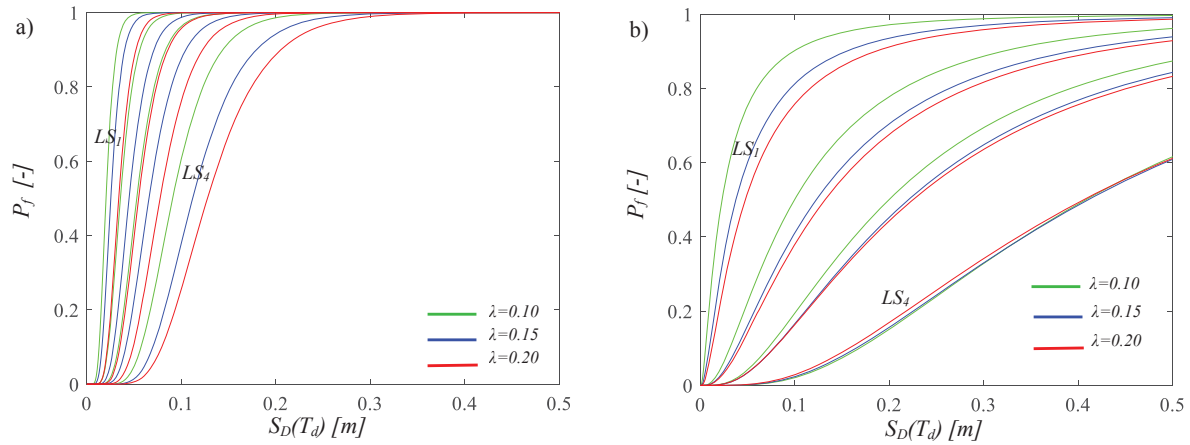

Figure 4: Seismic fragility curves of the pier for T_p=0.20s and T_d=1s (a), T_d=4s (d).

6 SEISMIC RELIABILITY OF ISOLATED BRIDGES WITH SINGLE CONCAVE FPS DEVICES

Adopting the Poisson model, the seismic reliability in 50 years can be computed by integrating the seismic fragility curves with the seismic hazard curves, evaluated for the same *IM* and related to the specific site (L'Aquila (Italy)). This allows to obtain the seismic reliability of the isolated multi-span continuous deck bridges, equipped with single concave FPS bearings.

6.1 Site seismic hazard

The seismic hazard curves (Figure 5) related to the site under analysis (L'Aquila (Italy)) are herein presented in terms of $S_D(T_d)$, as function of the fundamental periods. Each curve refers to the average values (50^{th} percentile) of the annual rate $\overline{\lambda}_s$ exceeding the $IM=S_D(T_d)$. It is easy to observe that the seismic hazard increases with the increase of the isolated period.

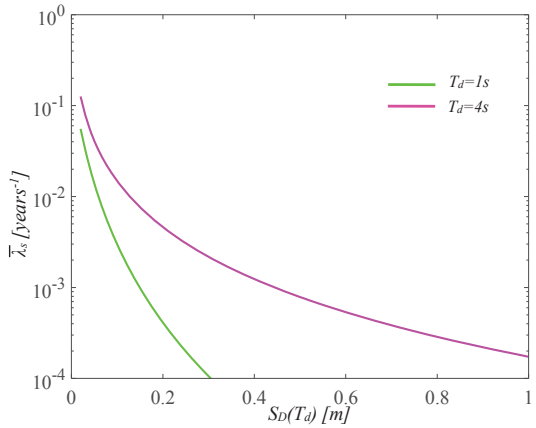

Figure 5: Seismic hazard curves in terms of $S_D(T_d)$ for the structural periods (T_d) related to L'Aquila site.

6.2 Seismic reliability curves

In the following, the seismic reliability curves for the pier (Figure 6) are reported for the different thresholds of *LS* as seen in the above Table 4. The limit states *LS1* and *LS2* are always respected demonstrating the effectiveness of the seismic isolation technique.

In addition, the "life safety" *LS3* is not always respected because of the very stringent (equal to 1/3 of the standard ones) limit states for the pier. Moreover, the most flexible RC

piers, with medium-high T_p values, exceed this *LS* also due to the aleatory uncertainty of the sliding friction coefficient. On the other hand, an increase in the vibration period of the FPS devices leads to an increase in seismic demand to the pier also due to the high seismic hazard of the site. Lower is the influence of the mass ratio.

The seismic reliability curves related to for the isolation system with respected to the pier (Figure 7). These reliability curves are almost linear and reveal that the isolation system is seismically less reliable as its fundamental period, T_d, increases, since higher and higher failure probabilities correspond to the same *LS* due to the high seismic hazard of the site. The other structural parameters have a reduced influence.

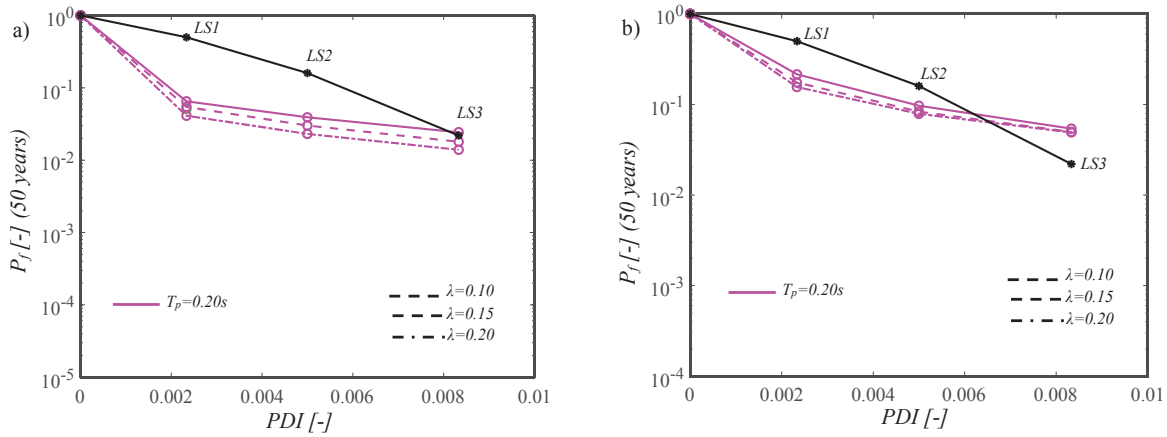

Figure 6: Seismic reliability curves of the pier for T_d=1s (a), T_d=4s (b).

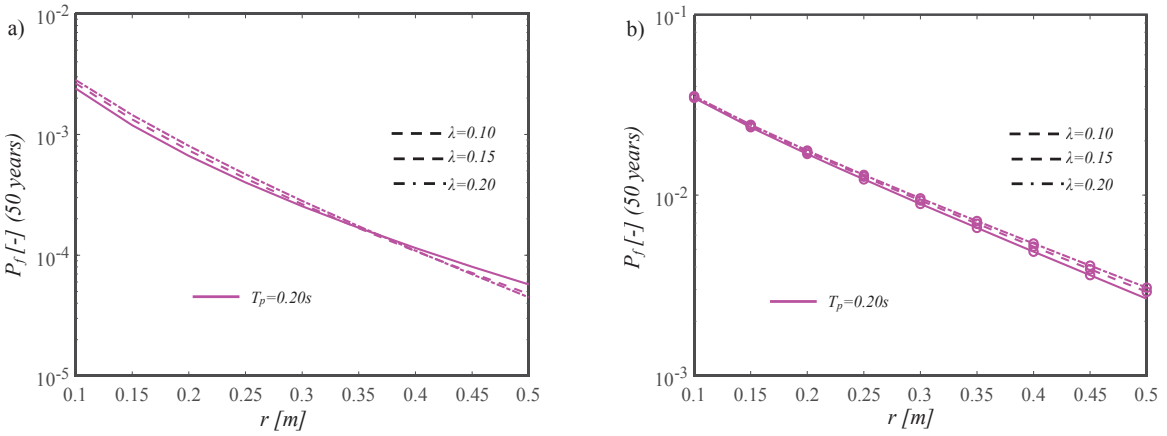

Figure 7: Seismic reliability curves of the deck response with respect to the pier for T_d=1s (a), T_d=4s (b).

7 CONCLUSIONS

This work regards the evaluation of the seismic reliability of multi-span continuous deck bridges isolated with single concave friction pendulum (FPS), accounting for a large range of isolator and bridge properties (i.e., the isolating system period, the vibration period of the elastic RC pier and the mass ratio, that is the ratio between the masses of the pier and the deck). A 6dof model is adopted, considering the RC pier flexibility, and both the RC abutment and RC deck infinitely rigid on the devices. The FP isolator is described by a widespread model, assuming that the friction coefficient varies with the velocity. The record-to-record is considered by defining a set of 30 ground motions, by scaling them to increasing seismic intensity levels. The fragility curves, referred both to the isolation system and the RC substructure/pier, have been computed for each limit state within the parametric analysis.

Then, the failure probabilities are evaluated considering the seismic hazard curves of the site (L'Aquila (Italy)), in a time interval of 50 years. This has resulted in the seismic reliability curves.

The seismic fragility of the seismic device decreases for lower values of the pier period and for increasing values of the isolated period, while the mass ratio has a reduced influence. For the pier, the fragility decreases for low pier periods, for increasing values of the mass ratio and for medium-high isolated periods.

The seismic reliability curves have shown that: it decreases for both higher pier periods and higher isolated periods due to the aleatory uncertainty of the sliding friction coefficient and to the high seismic hazard of the site, for the deck it decreases with the increase of the curvature radius of the isolator. For the pier, the fully operational and operational limit states are always respected demonstrating the effectiveness of the seismic isolation technique.

REFERENCES

[1] Jangid, R.S. (2004). Seismic Response of Isolated Bridges. *Journal of Bridge Engineering*, 9*(*2), 156-166.

[2] Jangid, R.S. (2008). Stochastic response of bridges seismically isolated by Friction Pendulum System. *Journal of Bridge Engineering*, *13*(4), 319-330.

[3] Chen, L. K., Jiang, L. Z., Qin, H. X., Zhang, N., Ling, L., Zhang, Q. H., Li, Q., & Cao, D. F. (2019). Nonlinear seismic assessment of isolated high-speed railway bridge subjected to near-fault earthquake scenarios. *Structure and Infrastructure Engineering*, *15*(11), 1529-1547.

[4] Troisi R., Alfano G. 2019. Towns as Safety Organizational Fields: An Institutional Framework in Times of Emergency. *Sustainability*, 11: 7025, 2019, doi:10.3390/su11247025.

[5] Troisi R., Alfano G. 2020. Firms'crimes and land use in Italy. An exploratory data anlysis. New Metropolitan Perspectives, International Symposium – 4th edition, 27-30 May 2020, pp 10.

[6] Zayas, V.A, Low, S.S., & Mahin, S.A. (1990). A simple pendulum technique for achieving seismic isolation. *Earthquake Spectra*, *6*(2), 317–33.

[7] Mokha, A., Constantinou, M.C., & Reinhorn, A.M. (1990). Teflon Bearings in Base Isolation. I: Testing. *Journal of Structural Engineering*, *116*(2), 438-454.

[8] Constantinou, M.C., Mokha, A., & Reinhorn, A.M. (1990) Teflon Bearings in Base Isolation. II: Modeling. *Journal of Structural Engineering*, *116*(2), 455-474.

[9] Constantinou, M.C., Whittaker, A.S., Kalpakidis, Y., Fenz, D.M., & Warn, G.P. (2007). Performance of Seismic Isolation Hardware Under Service and Seismic Loading. *Technical Report* MCEER-07-0012.

[10] Tsiavos, A., Schlatter, D., Markic, T., & Stojadinovic, B. (2017). Experimental and analytical investigation of the inelastic behavior of structures isolated using friction pendulum bearings, *Procedia Engineering*, 199, 465-470.

[11] Kunde, M. C., & Jangid, R. S. (2006). Effects of pier and deck flexibility on the seismic response of isolated bridges. *Journal of Bridge Engineering*, *11*(1), 109-121.

[12] Castaldo, P., Ripani, M., & Lo Piore, R. (2018). Influence of soil conditions on the optimal sliding friction coefficient for isolated bridges. *Soil Dynamics and Earthquake Engineering*, *111*, 131–148. https://doi.org/10.1016/j.soildyn.2018.04.056.

[13] Eröz, M., & DesRoches, R. (2013). The influence of design parameters on the response of bridges seismically isolated with the friction pendulum system (FPS). *Engineering structures*, *56*, 585-599.

[14] Castaldo, P., Amendola, G., & Palazzo, B. (2017). Seismic fragility and reliability of structures isolated by friction pendulum devices: Seismic reliability-based design (SRBD). *Earthquake Engineering and Structural Dynamics*, *46*(3), 425–446, DOI: 10.1002/eqe.2798.

[15] Castaldo, P., Palazzo, B., Alfano G., & Palumbo, M.F. (2018). Seismic reliability-based ductility demand for hardening and softening structures isolated by friction pendulum bearings. *Structural Control and Health Monitoring*, *25*(11), e2256. https://doi.org/10.1002/stc.2256

[16] Palazzo, B., Castaldo, P., & Della Vecchia, P. (2014, September). Seismic reliability analysis of base-isolated structures with friction pendulum system. In 2014 IEEE Workshop on Environmental, Energy, and Structural Monitoring Systems Proceedings (pp. 1-6). IEEE.

[17] Castaldo, P., Palazzo, B., Ferrentino, T., & Petrone, G. (2017). Influence of the strength reduction factor on the seismic reliability of structures with FPS considering intermediate PGA/PGV ratios. Composites Part B: Engineering, 115, 308-315.

[18] Castaldo, P., & Alfano, G. (2020). Seismic reliability-based design of hardening and softening structures isolated by double concave sliding devices. *Soil Dynamics and Earthquake Engineering*, *129*, 105930.

[19] Nassar, M., Guizani, L., Nollet, M. J., & Tahan, A. (2019). A probability-based reliability assessment approach of seismic base-isolated bridges in cold regions. *Engineering Structures*, *197*, 109353.

[20] Ghosh, S., Ghosh, S., & Chakraborty, S. (2018). Seismic reliability analysis of reinforced concrete bridge pier using efficient response surface method–based simulation. Advances in Structural Engineering, *21*(15), 2326-2339.

[21] Muntasir Billah, A. H. M., & Shahria Alam, M. (2015). Seismic fragility assessment of highway bridges: a state-of-the-art review. *Structure and Infrastructure Engineering*, *11*(6), 804-832.

[22] Avşar, Ö., & Özdemir, G. (2013). Response of seismic-isolated bridges in relation to intensity measures of ordinary and pulselike ground motions. *Journal of Bridge Engineering*, *18*(3), 250-260.

[23] Yanweerasak, T., Pansuk, W., Akiyama, M., & Frangopol, D. M. (2018). Life-cycle reliability assessment of reinforced concrete bridges under multiple hazards. *Structure and Infrastructure Engineering*, *14*(7), 1011-1024.

[24] Akiyama, M., Matsuzaki, H., Dang, H. T., & Suzuki, M. (2012). Reliability-based capacity design for reinforced concrete bridge structures. *Structure and Infrastructure Engineering*, *8*(12), 1096-1107.

[25] Wang, Yen-Po., Chung, Lap-Loi., & Liao, Wei-Hsin. (1998). Seismic response analysis of bridges isolated with friction pendulum bearings. *Earth. Eng. & Str. Dyn.*, *27*, 1069-1093.

[26] Kunde, M.C., & Jangid, R.S. (2003). Seismic behavior of isolated bridges: A-state-of-the-art review. *Electronic Journal of Structural Engineering,* 3.

[27] Celarec, D., & Dolšek, M. (2013). The impact of modelling uncertainties on the seismic performance assessment of reinforced concrete frame buildings. *Engineering Structures*, *52*, 340-354.

[28] Vamvatsikos, D., & Cornell, C.A. (2002). Incremental dynamic analysis. *Earthquake Engineering and Structural Dynamics*, *31*(3), 491–514.

[29] Cornell, C.A., & Krawinkler, H. (2000). Progress and challenges in seismic performance assessment. *PEER Center News*, *4*(1), 1-3.

[30] Bertagnoli, G., Mancini, G., Tondolo, F. Early age cracking of massive concrete piers, *Magazine of Concrete Research*, 2011, 63, 10, 1, 723-736.

[31] Bertagnoli G., Giordano L., Mancini S. Design and optimization of skew reinforcement in concrete shells, *Structural Concrete*, 2012, 13, 4, 248-258.

[32] Bertagnoli G., Giordano L., Mancini, S. Optimization of concrete shells using genetic algorithms, *ZAMM Zeitschrift fur Angewandte Mathematik und Mechanik*, 2014, 94, 1-2, 43-54.

[33] Mancini G., Carbone V.I., Bertagnoli G., Gino, D. Reliability-based evaluation of bond strength for tensed lapped joints and anchorages in new and existing reinforced concrete structures, *Structural Concrete*, 2018, 19, 3, 904-917.

[34] Bertagnoli G., Gino D., Martinelli, E. A simplified method for predicting early-age stresses in slabs of steel-concrete composite beams in partial interaction, *Engineering Structures*, 2017,140, 286-297.

[35] Porter, K.A. (2003). An overview of PEER's performance-based earthquake engineering methodology. *Proceedings of the 9th International Conference on Application of Statistics and Probability in Civil Engineering* (*ICASP9*), San Francisco, California.

[36] Aslani, H., & Miranda, E. (2005) Probability-based seismic response analysis. *Engineering Structures*, *27*(8), 1151-1163.

[37] PEER, *Pacific Earthquake Engineering Research Center* http://peer.berkeley.edu/

[38] ITACA, *Italian Accelerometric Archive* http://itaca.mi.ingv.it/ItacaNet/itaca10_links.htm

[39] ISESD, *Internet-Site for European Strong-Motion Data* http://www.isesd.hi.is/ESD_Local/frameset.htm

[40] ATC-63. 2008. Quantification of building seismic performance factors. FEMAP695. Redwood City, CA.

[41] Shome, N., Cornell, C.A., Bazzurro, P., & Carballo, J.E. (1998). Earthquake, records, and nonlinear responses. *Earthquake Spectra*, *14*(3), 469-500.

[42] Pinto, P.E., Giannini, R., & Franchin, P. (2003). Seismic Reliability Analysis of Structures, *IUSS Press*, Pavia, Italy.

[43] Luco, N., & Cornell, C.A. (2007). Structure-specific scalar intensity measures for near-source and ordinary earthquake ground motions. *Earthquake Spectra*, *23*(2), 357-92.

[44] NTC18. Norme tecniche per le costruzioni. Gazzetta Ufficiale del 20.02.18, DM 17.01.18, Ministero delle Infrastrutture.

[45] Iervolino, I., & Cornell, C.A. (2005). Record selection for nonlinear seismic analysis of structures. *Earthquake Spectra*, *21*(3), 685-713.

[46] Ryan, K., Chopra, A. (2004). Estimation of Seismic Demands on Isolators Based on Nonlinear Analysis. *Journal of Structural Engineering*, *130*(3), 392–402.

[47] Wei, B., Fu, Y., Li, S., Jiang, L., & He, W. (2020). Scaling errors of a seismic isolation system with a shear key. *Soil Dynamics and Earthquake Engineering*, *139*, 106382.

[48] Math Works Inc. (1997) MATLAB-High Performance Numeric Computation and Visualization Software: User's Guide. Natick, MA, USA.

[49] Garzillo C., Troisi R. Le decisioni dell'EMA nel campo delle medicine umane. In EMA e le relazioni con le Big Pharma - I profili organizzativi della filiera del farmaco, G. Giappichelli, 85-133, 2015.

[50] Golzio L. E., Troisi R. The value of interdisciplinary research: a model of interdisciplinarity between legal re-search and research in organizations. *Journal For Development And Leadership*, 2: 23-38, 2013.

[51] Nese A., Troisi R. Corruption among mayors: evidence from Italian Court of Cassation judgments, *Trends In Organized Crime*, 1-26, 2018. DOI:10.1007/s12117-018-9349-4.

[52] Troisi R., Golzio, L. E. Legal studies and organization theory: a possible cooperation. *Manageable cooperation* - European Academy of Management: 16th EURAM Conference, Paris, 1-2, 1-4 June 2016.

[53] Troisi R., Guida V. Is the Appointee Procedure a Real Selection or a Mere Political Exchange? The Case of the Italian Health-Care Chief Executive Officers. *Journal of Entrepreneurial and Organizational Diversity*, 7 (2): 19-38, 2018, DOI:10.5947/jeod.2018.008.

[54] De Iuliis, M., & Castaldo, P. (2012). An energy-based approach to the seismic control of one-way asymmetrical structural systems using semi-active devices. Ingegneria Sismica-International Journal of Earthquake Engineering, 29(4), 31-42.

[55] Basone, F., Castaldo, P., Cavaleri, L., & Di Trapani, F. (2019). Response spectrum analysis of frame structures: reliability-based comparison between complete quadratic combination and damping-adjusted combination. Bulletin of Earthquake Engineering, 17(5), 2687-2713.

[56] Troisi R. Le risorse umane nelle BCC: lavoro e motivazioni al lavoro. In Progetto aree bianche. Il sistema del credito cooperativo in Campania, 1: 399-417, 2012.

[57] SEAOC Vision 2000. 1995. Committee. Performance-based seismic design engineering. Report prepared by Structural Engineers Association of California, Sacramento, CA.

[58] Building Seismic Safety Council. 1997. NEHRP commentary on the guidelines for the seismic rehabilitation of buildings. Provisions (FEMA 274), Washington, DC.